OXFORD

Incorporating boron distribution variations in microdosimetric kinetic model-based relative biological effectiveness calculations for boron neutron capture therapy

Mingzhu Li[1,2], **Changran Geng**[1,2,*] ⓘ, **Yang Han**[1,2], **Fada Guan**[3], **Yuanhao Liu**[1,2,4], **Diyun Shu**[1,2,4], **Xiaobin Tang**[1,2]

[1]Department of Nuclear Science and Technology, Nanjing University of Aeronautics and Astronautics, Nanjing, 211106, China
[2]Joint International Research Laboratory on Advanced Particle Therapy, Nanjing University of Aeronautics and Astronautics, Nanjing, 211100, China
[3]Department of Therapeutic Radiology, Yale University School of Medicine, New Haven, Connecticut, 06530, United States
[4]Neuboron Medtech Ltd., Nanjing, Jiangsu, 211112, China

*Corresponding author. Department of Nuclear Science and Technology, Nanjing University of Aeronautics and Astronautics, Nanjing, 211106, China. E-mail: gengchr@nuaa.edu.cn

Abstract

This study introduces the MKM_B model, an approach derived from the MKM model, designed to evaluate the biological effectiveness of Boron Neutron Capture Therapy (BNCT) in the face of challenges from varying microscopic boron distributions. The model introduces a boron compensation factor, allowing for the assessment of compound Biological Effectiveness (CBE) values for different boron distributions. Utilizing the TOPAS simulation platform, the lineal energy spectrum of particles in BNCT was simulated, and the sensitivity of the MKM_B model to parameter variations and the influence of cell size on the model were thoroughly investigated. The CBE values for ^{10}B-boronphenylalanine (BPA) and ^{10}B-sodium (BSH) were determined to be 3.70 and 1.75, respectively. These calculations were based on using the nucleus radius of 2.5 μm and the cell radius of 5 μm while considering a 50% surviving fraction. It was observed that as cell size decreased, the CBE values for both BPA and BSH increased. Additionally, the model parameter r_d was identified as having the most significant impact on CBE, with other parameters showing moderate effects. The development of the MKM_B model enables the accurate prediction of CBE under different boron distributions in BNCT. This model offers a promising approach to optimize treatment planning by providing increased accuracy in biological effectiveness.

Introduction

Boron neutron capture therapy (BNCT) is an advanced binary targeted radiotherapy that is based on the ^{10}B(n,α)^{7}Li capture reaction. The energies of the released alpha particle and ^{7}Li ion are low, so they have very short penetration ranges (<10 μm in human tissue) and very high linear energy transfer (LET) of >100 keV/μm [1, 2]. As such, alpha particle and ^{7}Li ion can deposit most of their energies locally. The characteristics of short range and high LET have made BNCT highly effective against locally invasive malignancies. From the perspective of radiobiology, the relative biological effectiveness (RBE) of BNCT should be greater than unity compared with the conventional photon-based radiation therapy [2–4]. However, accurately estimating the clinical RBE of BNCT is challenging. For example, the therapeutic effects of BNCT have been observed to be dependent on the spatial distribution and concentration of boron within tumor cells [5]. Different from the straightforward RBE concept applied in other charged particle therapy, such as proton and carbon ion external beam radiotherapy,

the concept of compound biological effectiveness (CBE), proposed by Morris *et al*., is usually used to estimate the biological effectiveness of BNCT for different boron compounds [6, 7].

The values of CBE in BNCT can be determined from biological experiments or mathematical modeling. Many previous studies have utilized data from animal experiments to estimate the biological effectiveness of different types of boron compounds in BNCT. The most commonly used clinical boron drugs are ^{10}B-boronphenylalanine (BPA: $C_9H_{12}BNO_4$) and ^{10}B-sodium (BSH: $Na_2B_{12}H_{11}SH$). One experimental study by Suzuki *et al*. has shown that the CBEs of BSH and BPA in tumors were 0.94 and 4.25, respectively, at 50% surviving fraction [6, 8–10]. Different phenomenological and mechanistic models have been developed to calculate the biological effectiveness of charged particles. In addition to absorbed dose, the stochastic physical quantities in microdosimetry, such as lineal energy y and specific energy z, are commonly used in the biophysical modeling for heavy charged particles. For example, Horiguchi *et al*. have applied the microdosimetric kinetic model (MKM) proposed by Hawkins to estimate the alpha in the linear–quadratic (LQ) model of cell survival curve [11–14]. Hu *et al*. have recently applied the Monte Carlo simulation tool PHITS in microdosimetry studies and evaluated the biological effectiveness and absorbed doses of BNCT [15]. A modeling study by Sato *et al*. found that the probability density function of lineal energy y, denoted as $f(y)$, obtained by different boron drugs is close to one another, and the frequency-mean lineal energy ($\bar{y}_F$) values for BPA and BSH at the micrometer level were 118.43 and 120.32 keV/μm, respectively. However, the experimental data from Fukuda *et al*. have shown that the different microscopic boron distributions with the same macro-concentration could have a considerable effect on CBE [16]. This discrepancy has urged Sato *et al*. to modify their modeling work. They used the stochastic microdosimetric kinetic model (SMK) instead of the early MKM. However, their results are difficult to reproduce, and their calculation results were biased toward higher values [17].

In this study, a new MKM-based mathematic model, denoted as MKM_B model, was proposed by introducing a boron compensation factor that takes into account different micro-distributions of boron compounds to evaluate the CBE of BNCT. For testing the feasibility of the MKM_B model, the parameters $f(y)$ and $\bar{y}_F$ were obtained through TOPAS, and the calculated results for CBE were compared with experimental values. Then, different cell sizes and the influence of input parameters in the MKM_B model were simulated to explore their effect on CBE.

Materials and methods
Principle of MKM_B model

MKM is one of the biophysical models for evaluating biological effectiveness, with the endpoint of clonogenic cell survival. It is based on the theory of dual radiation action, which was first proposed by Kellerer *et al*. [18]. In accordance with the LQ relation, the cellular surviving fraction, S, at the dose D is calculated as follows:

$$S = \exp\left(-\alpha D - \beta D^2\right), \qquad (1)$$

where the parameters α and β are the linear and quadratic coefficients, respectively. The CBE (the same as RBE) of charged particles for the cell survival fraction, S, can be calculated as follows:

$$RBE(S) = \frac{D_\gamma(S)}{D(S)} = \frac{\frac{-\alpha_\gamma + \sqrt{\alpha_\gamma^2 - 4\beta_\gamma \ln(s)}}{2\beta_\gamma}}{\frac{-\alpha + \sqrt{\alpha^2 - 4\beta \ln(s)}}{2\beta}}, \qquad (2)$$

where $D(S)$ and $D_\gamma(S)$ represent the absorbed dose for the radiation of interest and reference radiation, respectively, at the same S. The parameters α_γ and β_γ are usually obtained experimentally from the survival curve of cells irradiated by reference photon radiation such as X-rays or gamma rays. The β parameter is assumed to be constant in the MKM among different radiations [19, 20]. The value of α can be estimated from β by considering Poisson distribution and the overkill effect as follows [21]:

$$\alpha = \alpha_0 + \beta z_{1D}^*, \qquad (3)$$

where α_0 is a constant that represents the initial slope of the survival curve in the limit of LET equal to zero. The parameter z_{1D}^* denotes the saturation-corrected dose-mean specific energy [22], and it is calculated as follows:

$$z_{1D}^* = \frac{\bar{l}}{m} y^* \equiv \frac{1}{\rho \pi r_d^2} \frac{y_0^2 \int \left[1 - \exp\left(-\frac{y^2}{y_0^2}\right)\right] f(y) dy}{\int y f(y) dy}, \qquad (4)$$

where y is the ratio of energy imparted [ε_s; i.e. energy deposition in sensitive volume (SV) for every single event s] and the mean chord length ($\bar{l}$; i.e. 2/3 of the SV diameter) in SV, with m representing the mass of the SV. The saturation-corrected dose-mean lineal energy, y^*, is calculated using the right part of Equation (4). The saturation parameter y_0 is a threshold value, above which the cell overkill effect appears.

The assumptions of the MKM_B model are described as follows. In the LQ formula, the dose considered is the macroscopic average dose. However, for BNCT, due to the different distributions of boron drugs and the short range of the released secondary charged particles, even with the same average dose, the nucleus dose, which strongly depends on the local distribution of boron drugs, received by the cell nucleus (radiosensitive region) may not be equal to the average dose. Moreover, different boron drugs exhibit different physiological behavior in tumors, causing different spatial distributions and thus resulting in different biological effectiveness. A boron compensation factor (f_B), was introduced to compensate the discrepancy between local dose and average dose, and it is calculated as follows:

$$f_B = D_{nucleus\ dose} / D_{macroscopic\ average\ dose} \qquad (5)$$

which is defined as the ratio of the nucleus dose received by the nucleus ($D_{nucleus\ dose}$) and the macroscopic average dose ($D_{macroscopic\ average\ dose}$), both of which are simulated.

The LQ formula for the MKM_B model is then rewritten as follows:

$$S = \exp\left(-\alpha f_B D - \beta f_B^2 D^2\right). \qquad (6)$$

Lineal energy calculation
Monto Carlo simulation toolkit
The Monte Carlo simulation toolkit TOPAS was used in this study. TOPAS is known for its versatile applications in radiation physics and dosimetry, focusing on accurately simulating particles across various scales. The specific physics model employed in the study is G4EmLivermorePhysics (step size = 0.01 μm). This model provides a precise description of electromagnetic physics processes in the low-energy domain [23–25]. In terms of the simulation parameters, a total of 2×10^8 were used in the present study to ensure enough uncertainties as in previous studies [26–28].

Geometry models
A $3 \times 3 \times 3$ cell array was constructed in the Monte Carlo simulation (Figure 1). Each cell comprises a membrane, a cytoplasm, and a nucleus. The default nucleus and cellular radius were set to 2.5 and 5 μm, respectively, and the cell membrane thickness was set to 8 nm. To ensure that the effects of neighboring cells have been taken into account, we implemented volume sources within each cell. However, lineal energy counting was performed only in the central cell nucleus. The material of the cell was simply assumed to be water.

Particle source
Particle sources with varying spatial distributions were developed considering the original processes and ranges of particles involved in BNCT. According to the experiment data [29], boron drugs are mainly present in the cytoplasm, cell membrane, and extracellular spaces, and the range of alpha and ^{7}Li particles produced in BNCT is approximately within the cell. Therefore, three isotropic particle source patterns were established in the Monte Carlo simulations: uniformly enriched in the extracellular space (Ic), cytoplasm (Cy), and cell membrane (Cm). The alpha particles in BNCT had energy levels of 1.47 (93.7%) and 1.77 MeV (6.3%), and their spatial distribution primarily depended on the microscopic distribution of boron drugs but was not related to the incident neutron fluence rate, which is approximately constant at the sub cellular level. Meanwhile, the energy levels of ^{7}Li ions are 1.02 (6.3%) and 0.84 MeV (93.7%), and their spatial distribution is similar to that of alpha particles because of their short ranges at the cellular scale.

Lineal energy analysis
Lineal energy (y) is defined as the ratio of energy imparted (ε) (i.e. energy deposition in SV for each event) and the mean chord length (l) (i.e. 2/3 of the SV diameter) in SV. The lower and upper limits of lineal energy were set to 0.1 and 10 000 keV/μm (step size = 0.01 μm), respectively. Figure 2 shows the schematic of lineal energy calculation. The counting area is in the central nucleus. The lineal energy spectrum was determined by the processes proposed in Kyriakou et al. [30].

(1) Let an event s be defined as a primary particle and all its secondary particles;

(2) Randomly sample one energy deposition('hit');

(3) The SV is randomly placed at a distance from this hit less than the sensitive radius (r_d);

(4) Calculate the energy deposition in the SV and determine the lineal energy with the associated statistical weight;

Given that $f(y)$ is the probability function of the lineal energy y, the frequency-mean lineal energy ($\bar{y}_F$) can be calculated as follows:

$$\bar{y}_F = \int_0^\infty y f(y) dy, \qquad (7)$$

Assuming that the boron drug is unable to penetrate the nucleus [16], the incidence of ions entering the nucleus can be considered as independent events. Meanwhile, due to the different distribution of boron, the microscopic boron distribution must be weighed. The lineal energy frequency of the compound particles ($f(y)^j$) is thus determined by Equation (8) as

follows:

$$f(y)^j \quad = \frac{\sum_{i,k} M_k^i Q^{i,j} f(y)_k^i}{\sum_{i,k} M_k^i Q^{i,j}}, \tag{8}$$

where M is the fraction of initial primary ions that reach the counting area and deposit energy within the SV, along with the boron distribution factor Q; i refers to the source condition (i.e. Ic, Cy, and Cm); j represents the boron distribution (i.e. BPA and BSH); and k refers to the particle type (i.e. alpha and ^{7}Li). The $f(y)_k^i$ undergoes normalization. In practice, the ratios of ^{10}B concentrations in intra- and extracellular regions are ~3.2 for BPA and 0.86 for BSH [31]. On the basis of the boron concentration data of malignant tumor cells [31] and the cell size [16], the Q values are listed in Table 1.

CBE analysis

Model parameters

The model parameters were set as 0.13 Gy^{-1} for α_0, 0.05 Gy^{-2} for β, 150 keV/μm for y_0, 0.42 μm for r_d on the basis of previous studies in human salivary grand (HSG) tumor cells [21, 32]. In the present study, $\alpha_\gamma = 0.19$ Gy^{-1} and $\beta_\gamma = 0.05$ Gy^{-2} were used as the parameters of the reference radiation (200 kVp X-rays) for calculating the CBE.

Input parameters for sensitivity analysis

To quantify and evaluate the influence of input parameters in the MKM_B model on the CBE results, a sensitivity study was conducted. The cell (cell radius 3 μm, nucleus radius of 1.5 μm; cell radius 4 μm, nucleus radius of 2 μm; cell radius 5 μm, nucleus radius of 3 μm) in different simulations was varied to investigate their effects on biological effectiveness by using the MKM_B model. A single-parameter variation study of the model parameters was conducted by varying the parameters separated by $\pm$ (5%, 25%, 50%) of the nominal values, When investigating the impact of r_d on CBE, r_d was utilized as the radius of the SV for simulation, and the CBE under different conditions was finally obtained [33].

Results

Lineal energy distribution of secondary particles

The lineal energy spectra of alpha and ^{7}Li particles are presented in Fig. 3. The boron distribution factor (Q) is presented in Table 1.

The lineal energy distributions under different source conditions are similar for alpha particles (Fig. 3a).

Table 1. Boron distribution factor for Equation (8).

		BPA	BSH
Q	Ic	0.2214	0.5141
	Cy	0.7786	
	Cm		0.4859

The observation could be attributed to the fact that the alpha particles generated in BNCT have a longer range (8–10 μm) and are capable of penetrating the cytoplasm and nucleus more effectively. Therefore, the alpha particles have a wide energy range when they reach the nucleus, leading to a more consistent distribution of ionization capacity and lineal energy.

However, differences in the linear energy spectra were observed under different source conditions for ^{7}Li particles, because the range of ^{7}Li particles was only about 3 μm. They were unable to penetrate the cytoplasm and nucleus, thus inducing a lower energy deposition in the nucleus under the Ic and Cm conditions. The frequency spectra of lineal energy (Fig. 3b) show that the lineal energy is more concentrated at the high-y region under the Cy condition, resulting in a higher $\bar{y}_F$ than the Cm and Ic conditions. This difference is because the ^{7}Li particles emitted under the Cy condition are closer to the nucleus, resulting in a higher residual energy and ionization capacity when they reach the nucleus. Table 2 shows that the law of $\bar{y}_F$ and $\bar{y}_D$ for alpha particles still obeys $Cy > Cm > Ic$, the same as for ^{7}Li.

Compound biological effectiveness

In the concept of CBE, the compound effect specifically refers to the boron compound effect because of the inhomogeneous distribution of the boron compounds. The lineal energy spectra (frequency) of the compound particles (alpha $+^7$Li) for BPA and BSH are compared in Fig. 4a. The survival curves of HSG tumor cells from the reference X-rays, BNCT with BPA, and BNCT with BSH are compared in Fig. 4b.

The calculated frequency-mean lineal energy values from Fig. 4a were 154.89 and 125.11 keV/μm for BPA and BSH in BNCT, respectively. Notably, the lineal energy spectral distribution of the compound particles shown in Fig. 4a is similar to that of 'pure alpha' (shown in Fig. 3), because alpha particles have a longer range (~10 μm) than ^{7}Li particles (~3 μm). Alpha particles can also penetrate the cytoplasm much more accessibly, which enables them to comprise the central portion of the compound particles within the nucleus. The disparity observed in the $yf(y)$ diagram between BPA and BSH primarily arises from the presence of ^{7}Li. In the BPA condition, the emission site of ^{7}Li

Table 2. Frequency-mean lineal energy ($\bar{y}_F$) and dose-mean lineal energy ($\bar{y}_D$) of alpha and ^{7}Li in BNCT.

	Alpha		Lithium	
	$\bar{y}_F$(keV/μm)	$\bar{y}_D$(keV/μm)	$\bar{y}_F$(keV/μm)	$\bar{y}_D$(keV/μm)
Cy	191.33 ± 12.5	231.79 ± 19.4	183.32 ± 3.23	260.40 ± 5.66
Cm	173.60 ± 10.5	217.72 ± 17.7	69.23 ± 0.95	101.93 ± 1.81
Ic	141.06 ± 4.39	187.40 ± 7.69	59.60 ± 0.85	91.18 ± 1.87

Table 3. Intermediate parameter results of BPA and BSH in MKM_B model.

	$\bar{y}_F$ (keV/μm)	$\bar{y}_D$ (keV/μm)	y^* (keV/μm)	z_{1D}^* (Gy)	α^* (Gy^{-1})	D(Gy)
BPA	192.65	238.09	79.35	22.91	1.28	0.84
BSH	148.30	194.32	81.87	23.64	1.31	0.40
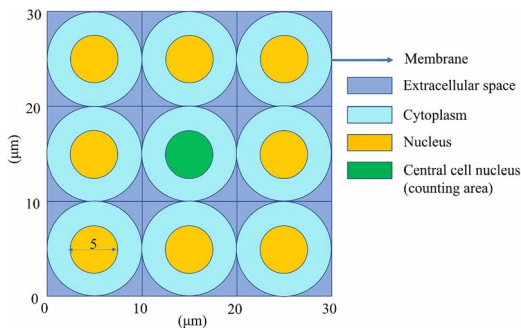
Figure 1. Cross-sectional view of the geometric model.

Figure 2. Schematic of lineal energy calculation; the volumes of SVs and nucleus are for visual display and do not represent the actual size.

Table 4. CBE results of BPA and BSH in the MKM_B model.

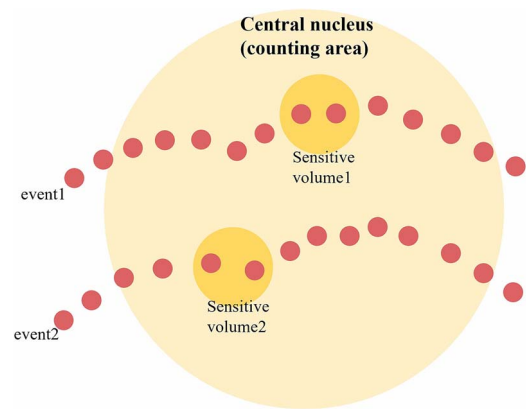|	CBE(BPA)	CBE(BSH)
This work (10% surviving fraction)	2.55	1.24
This work (50% surviving fraction)	3.60	1.77
Currently used value for tumor in treatment planning system [34–37]	3.8	2.5
Liver tumors (37% surviving fraction) [10]	4.25	0.94
SCC VII murine squamous cell carcinoma -PHITS simulation (50% surviving fraction) [16]	5.49	3.55

particles is closer to the nucleus, leading to a reduction in its short range. Consequently, ^{7}Li particles exert a more pronounced influence. This effect is reflected in Fig. 3b, where a concentration of counts at a higher lineal energy region was observed for BPA.

The lineal energy frequency spectrum can be substituted into the MKM_B model and solved for the intermediate parameters appearing in the model. Table 3 presents the intermediate parameter results, including the $\bar{y}_F$, $\bar{y}_D$ y^*, z_{1D}^*, α, and f_B. In the calculation of f_B, the same configuration was used as shown in Fig. 1. The $D_{macroscopic\ average\ dose}$ is determined by scoring the dose in the central cube, while the $D_{nucleus\ dose}$ is scored as the dose in the nucleus of the central cell. Subsequently, f_B is computed based on Equation (5). The survival fraction curve can be obtained by changing D, as shown in Fig. 4b.

The CBE is obtained by the value of D_γ in the reference radiation (X-rays) divided by D under the same survival fraction S. Table 5 presents the f_B and CBE results. The CBE values provided in Table 4 for tumor is widely utilized in treatment planning systems. The results of the current work agree well with the CBE values of treatment planning system and experimental data in literature [10, 33–38].

Sensitivity analysis of input parameters

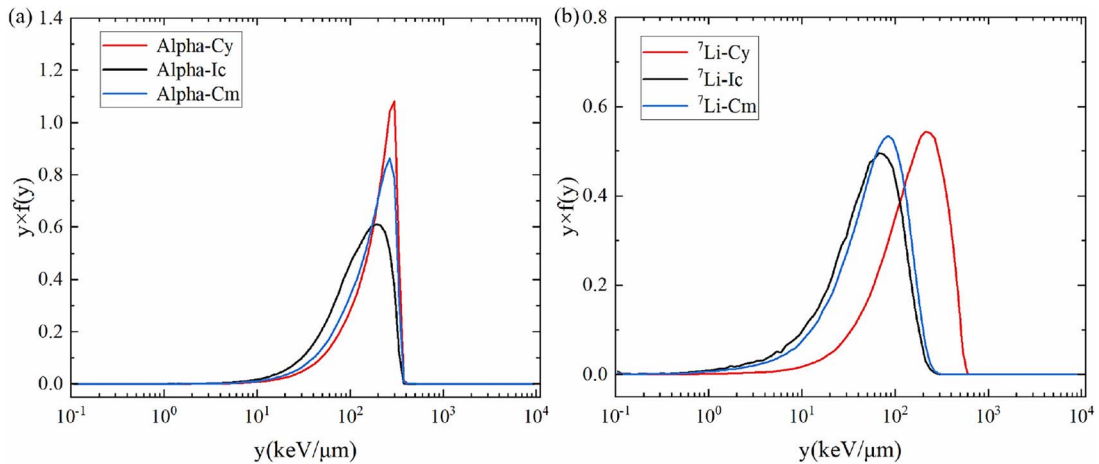The impact of varying cell sizes (the cell shape remains constant) of the MKM_B model on CBE is summarized

Figure 3. Frequency spectra of lineal energy for (a) alpha and (b) ^{7}Li particles; solid lines with different colors represent the spectra under different source conditions.
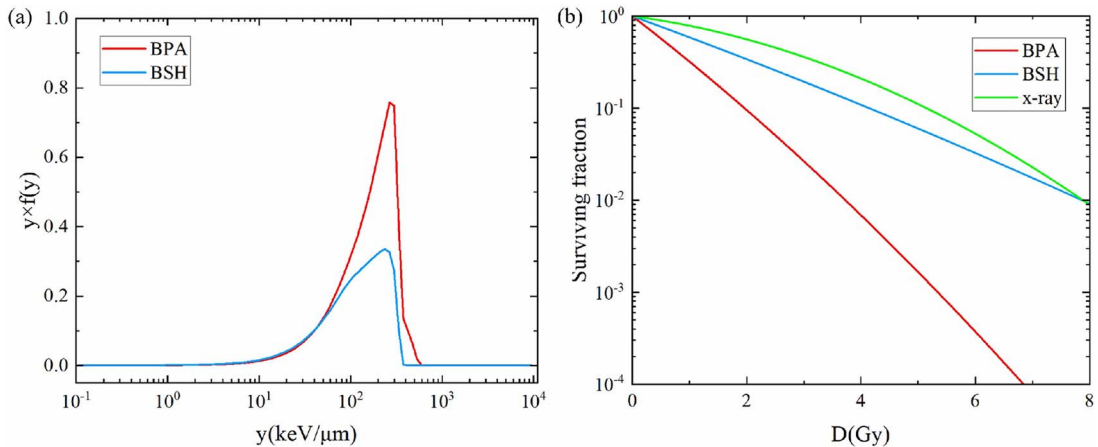

Figure 4. (a) Lineal energy spectra (frequency) of compound particles (alpha +^{7}Li) in BNCT; (b) calculated cell survival curves of HSG tumor cells.

in Table 5. The results showed the effect of different cell sizes on f_B and CBE results, which demonstrated that when the cell radius was decreased by 1 μm and the nucleus radius was decreased by 0.5 μm, the f_B value of BPA increased by ∼0.05, and the BSH was about 0.1. However, when only the nucleus radius was decreased by 0.5 μm, the f_B values of BPA increased by about 0.05, the f_B value of BSH decreased by about 0.05. The trend of CBE changes was consistent with that of f_B. The effects of varying the model parameters (the cell shape and sizes remains constant) of the MKM_B model on CBE are presented in Fig. 5. Figure 5a illustrates that the CBE difference [%] for BPA (BSH is the same as BPA) under the parameters changed by ± (5%, 25%, 50%) and Fig. 5b depicts the corresponding CBE values. The results indicated that the value of r_d had the greatest effect on the calculated

CBE values. Meanwhile, changes in the parameters α_0 and y_0 demonstrated minimal influence on the CBE values. Regardless of the variations in α_0, the calculated CBE values remained nearly constant. These findings provide valuable insights into the effect of parameter variations on the performance of the MKM_B model in drug discovery applications.

Discussion

Accurate dose assessment and determination of the biological effectiveness of BNCT are challenging because of the complicated radiation types and energy distribution at the micro- and nanometer scales [39]. The RBE calculation model MKM for conventional particles may not be appropriate to be directly applied in BNCT because the boron atoms are not uniformly
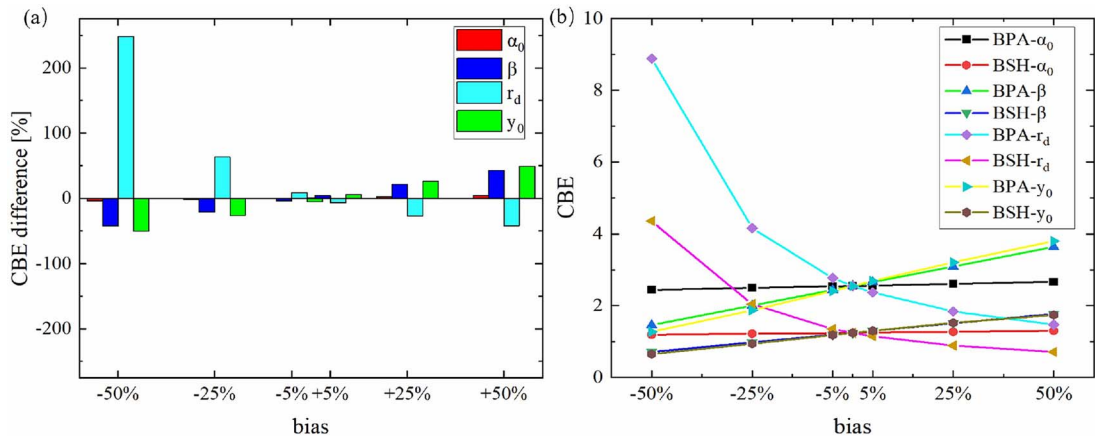
Figure 5. As the model parameters change CBE values for the boron drugs (BPA and BSH) with parameters changed separately by ± (5%, 25%, 50%) in BNCT: (a) CBE difference [%] for BPA; (b) CBE values.

Table 5. f_B values and CBE results of BPA and BSH in the MKM_B model for different cell sizes.

	Cell radius (μm)	Nucleus radius (μm)	f_B(BPA)	f_B(BSH)	CBE(BPA)	CBE(BSH)
10% surviving fraction	3	1.5	0.93	0.59	2.80	1.84
	4	2	0.88	0.49	2.66	1.52
	5	2.5	0.84	0.40	2.55	1.24
	5	3	0.80	0.43	2.43	1.34
50% surviving fraction	3	1.5	0.93	0.59	3.94	2.60
	4	2	0.88	0.49	3.75	2.15
	5	2.5	0.84	0.40	3.60	1.77
	5	3	0.80	0.43	3.42	1.89

distributed at the cellular scale. Although Sato *et al.* constructed the SMK model by taking into account the distribution of nucleus specific energy on the basis of the MKM, a notable detail that the SMK model involves a complex program and is challenging to reproduce, and the calculation of CBE results tend to be higher values [16]. In the present study, a novel MKM-based (MKM_B) model for CBE calculation in BNCT was proposed. The developed MKM_B model considers the effect of boron distribution caused by different boron drugs on the calculated CBE. As the accuracy of the applied CBE model and its input parameters may influence the delivery of homogeneous CBE-weighted dose to the target volume, a sensitivity study was conducted on the input parameters.

The lineal energy frequency spectrum of HSG tumor cells was explored [21] to examine the emitted alpha and ^{7}Li particles at various positions as well as the compound particles. The results indicated that the lineal energy frequency spectra of alpha particles emitted at different positions were almost consistent, whereas those of ^{7}Li particles showed large differences. Moreover, the lineal energy frequency spectrum of compound particles was similar to that of 'pure alpha' (Fig. 3), as alpha particles have a longer range (~10 μm) than ^{7}Li particles (~3 μm) and are more capable of penetrating the cytoplasm. Although the dose distributions of lineal energy and dose-mean lineal energy have been studied in our previous research [26], this article focus on the main parameter of the MKM_B model and will not describe this part in detail.

By using the newly developed MKM_B model, cell survival curves that demonstrated the effectiveness of different radiations and boron drugs were obtained. The curves revealed that BPA had the highest slope, indicating its capability to kill a larger number of tumor cells at the same prescription dose. This finding agrees with the fact that the CBE of BPA was much greater than that of BSH. The f_B values of BPA and BSH were 0.84 and 0.40, respectively, whereas the CBE values were 3.70 and 1.75, respectively, at 50% surviving fraction. These CBE values are in close agreement with the CBE values of treatment planning system and the experimental measurements reported in an article [10].

The sensitivity analysis involved systematically varying the parameters of the MKM_B model and observing the corresponding changes in the calculated values of CBE. By conducting such an analysis, we can quantify and evaluate the extent to which each parameter influences the CBE results. This information is valuable for understanding the model's behavior, identifying critical parameters, and potentially optimizing the model's performance or refining the treatment planning process in BNCT. Therefore, sensitivity studies are important. In this study, the total dose is the same, all settings are under ideal conditions, the effect of cell size on the model was discussed, and then the effect of changes in input parameters related to cell type on the CBE calculation results was analyzed. Upon changing the size of cells, the overall size (cell and nucleus radii) of a cell decreased, and the f_B of BPA and BSH gradually increased, mainly because when the cell size changes, the alpha and ^{7}Li particles are more likely to enter the cell nucleus, leading to an increase in nucleus dose and ultimately resulting in an increase in CBE values. However, when only the nucleus radius is decreased, the f_B of BPA gradually increases. Meanwhile, due to the inability of BSH to enter the cell and its long distance from the cell nucleus, the dose delivered to the nucleus decreases, so its f_B gradually decreases. These findings suggested that the proposed model can accurately predict the effects of boron drugs on cells of varying sizes, providing valuable insights for BNCT. Therefore, when calculating CBE in practice, the influence of cell size should be taken into account and detailed simulations based on the actual situation of cells are needed to obtain more accurate results. As shown in Table 5, when the nucleus radius is 1.5 and the cell radius is 3, the calculated CBE results compared to default cell size have a better consistency with the values of CBE currently used in the treatment planning system. In addition, the effect of different input parameters on CBE was examined. The results showed that r_d had the most considerable influence on the results, especially for BPA. These results are consistent with the sensitivity analysis of MKM studied by Dahle *et al*. [20]. Therefore, the value of r_d and the size of cells are crucial in the calculation of CBE, and a more accurate CBE value could be obtained if the exact input parameters and cell size are inputted during patient treatment.

This study has limitations. The MKM does not take into account synergism between components, the impact may be considered in the future. Besides, the cell structure (such as cell size and shape) and drug enrichment can affect microscopic boron distribution. Therefore, the value of CBE could also change accordingly. The current simulation settings for the geometry and source are relatively idealized. Furthermore, only

HSG tumor cell was used in the calculations, whereas the experimental data in literature consisted of multiple types of cells. In future studies, multiple cell types could be simulated, and the experimental results could be compared.

Conclusion

In this study, a modified MKM-based (MKM_B) model was proposed to calculate the CBE values of BNCT by considering the microscopic boron distribution in cells. These CBE values are in close agreement with the recognized value used in the treatment planning of BNCT. In addition, the sensitivity analysis was performed on various parameters in the MKM_B model to assess their impact on the calculation results of CBE. Furthermore, this work has potential to be extended to radiopharmaceutical therapy, which is fundamentally similar to BNCT.

Conflict of interest

None declared.

Funding

References

1. Suzuki M. Boron neutron capture therapy (BNCT): a unique role in radiotherapy with a view to entering the accelerator-based BNCT era. *Int J Clin Oncol* 2020;**25**: 43–50. https://doi.org/10.1007/s10147-019-01480-4.

2. Moss RL. Critical review, with an optimistic outlook, on boron neutron capture therapy (BNCT). *Appl Radiat Isot* 2014;**88**:2–11. https://doi.org/10.1016/j.apradiso.2013.11.109.

3. Barth RF, Coderre JA, Vicente MG. *et al.* Boron neutron capture therapy of cancer: current status and future prospects. *Clin Cancer Res* 2005;**11**:3987–4002. https://doi.org/10.1158/1078-0432.CCR-05-0035.

4. Matsumoto Y, Fukumitsu N, Ishikawa H. *et al.* A critical review of radiation therapy: from particle beam therapy (proton, carbon, and BNCT) to beyond. *J Pers Med* 2021;**11**:825. https://doi.org/10.3390/jpm11080825.

5. Hopewell JW, Morris GM, Schwint AE, Coderre JA. The radiobiological principles of boron neutron capture therapy: a critical review. *Applied Radiation and Isotopes* 2011;**69**;1756–1759. https://doi.org/10.1016/j.apradiso.2011.04.019.

6. Morris GM, Coderre JA, Hopewell JW. *et al.* Response of the central nervous system to boron neutron capture irra-

diation: evaluation using rat spinal cord model. *Radiother Oncol* 1994a;**32**:249–55. https://doi.org/10.1016/0167-8140(94)90024-8.

7. Ono K. An analysis of the structure of the compound biological effectiveness factor. *J Radiat Res* 2016;**57**:i83–9. https://doi.org/10.1093/jrr/rrw022.

8. Farias RO, Bortolussi S, Menendez PR. *et al*. Exploring boron neutron capture therapy for non-small cell lung cancer. *Phys Med* 2014;**30**:888–97. https://doi.org/10.1016/j.ejmp.2014.07.342.

9. Morris GM, Coderre JA, Hopewell JW. *et al*. Response of rat skin to boron neutron capture therapy with p-boronophenylalanine or borocaptate sodium. *Radiother Oncol* 1994;**32**:144–53. https://doi.org/10.1016/0167-8140(94)90101-5.

10. Suzuki M, Masunaga SI, Kinashi Y. *et al*. The effects of boron neutron capture therapy on liver tumors and normal hepatocytes in mice. *Jpn J Cancer Res* 2000;**91**:1058–64. https://doi.org/10.1111/j.1349-7006.2000.tb00885.x.

11. Hawkins RB. A microdosimetric-kinetic theory of the dependence of the RBE for cell death on LET. *Med Phys* 1998;**25**:1157–70. https://doi.org/10.1118/1.598307.

12. Horiguchi H, Sato T, Kumada H. *et al*. Estimation of relative biological effectiveness for boron neutron capture therapy using the PHITS code coupled with a microdosimetric kinetic model. *J Radiat Res* 2015;**56**:382–90. https://doi.org/10.1093/jrr/rru109.

13. Hawkins RB. A microsimetric-kinetic model of cell death from exposure to ionizing radiation of any LET, with experimental and clinical applications. *Int J Radiat Biol* 1996;**69**:739–55. https://doi.org/10.1080/095530096145481.

14. Bianchi A, Selva A, Colautti P. *et al*. Microdosimetry with a sealed mini-TEPC and a silicon telescope at a clinical proton SOBP of CATANA. *Radiat Phys Chem* 2020;**171**:108730. https://doi.org/10.1016/j.radphyschem.2020.108730.

15. Hu N, Tanaka H, Takata T. *et al*. Evaluation of PHITS for microdosimetry in BNCT to support radiobiological research. *Appl Radiat Isot* 2020;**161**:109148. https://doi.org/10.1016/j.apradiso.2020.109148.

16. Fukuda H. Response of normal tissues to boron neutron capture therapy (BNCT) with (10)B-borocaptate sodium (BSH) and (10)B-paraboronophenylalanine (BPA). *Cells* 2021;**10**:2883. https://doi.org/10.3390/cells10112883.

17. Sato T, Masunaga S-I, Kumada H. *et al*. Microdosimetric modeling of biological effectiveness for boron neutron capture therapy considering intra- and intercellular heterogeneity in 10B distribution. *Sci Rep* 2018;**8**:988. https://doi.org/10.1038/s41598-017-18871-0.

18. Kellerer AM, Rossi HH. A generalized formulation of dual radiation action radiation. *Research* 1978;**75**:471–88. https://doi.org/10.2307/3574835.

19. Inaniwa T, Kanematsu N. Adaptation of stochastic microdosimetric kinetic model for charged-particle therapy treatment planning. *Phys Med Biol* 2018;**63**:095011. https://doi.org/10.1088/1361-6560/aabede.

20. Dahle T, Magro G, Ytre-Hauge K. *et al*. Sensitivity study of the microdosimetric kinetic model parameters for carbon ion radiotherapy. *Phys Med Biol* 2018;**63**:225016. https://doi.org/10.1088/1361-6560/aae8b4.

21. Yuki K, Kanai T, Yoshitaka M. *et al*. Microdosimetric measurements and estimation of human cell survival for heavy-ion beams. *Radiat Res* 2006;**166**:629–38. https://doi.org/10.1667/RR0536.1.

22. Griffiths HJR. Microdosimetry ICRU report 36. *Medical Physics* 1985. https://doi.org/10.1148/radiology.154.2.528.

23. Schuemann J, McNamara AL, Ramos-Mendez J. *et al*. TOPAS-nBio: an extension to the TOPAS simulation toolkit for cellular and sub-cellular radiobiology. *Radiat Res* 2019;**191**:125–38. https://doi.org/10.1667/RR15226.1.

24. Perl J, Shin J, Schümann J. *et al*. TOPAS: an innovative proton Monte Carlo platform for research and clinical applications. *Med Phys* 2012;**39**:6818–37. https://doi.org/10.1118/1.4758060.

25. Faddegon B, Ramos-Méndez J, Schuemann J. *et al*. The TOPAS tool for particle simulation, a Monte Carlo simulation tool for physics, biology and clinical research. *Phys Med* 2020;**72**:114–21. https://doi.org/10.1016/j.ejmp.2020.03.019.

26. Han Y, Geng C, D-Kondo JN. *et al*. Microdosimetric analysis for boron neutron capture therapy via Monte Carlo track structure simulation with modified lithium cross-sections. *Radiat Phys Chem* 2023;**209**:110956. https://doi.org/10.1016/j.radphyschem.2023.110956.

27. Qi J, Geng C, Tang X. *et al*. Effect of spatial distribution of boron and oxygen concentration on DNA damage induced from boron neutron capture therapy using Monte Carlo simulations. *Int J Radiat Biol* 2021;**97**:986–96. https://doi.org/10.1080/09553002.2021.1928785.

28. Zhao S, Geng C, Guo C. *et al*. SARU: a self-attention ResUNet to generate synthetic CT images for MR-only BNCT treatment planning. *Med Phys* 2022;**50**:117–27. https://doi.org/10.1002/mp.15986.

29. Michiue H, Sakurai Y, Kondo N. *et al*. The acceleration of boron neutron capture therapy using multi-linked mercaptoundecahydrododecaborate (BSH) fused cell-penetrating peptide. *Biomaterials* 2014;**35**:3396–405. https://doi.org/10.1016/j.biomaterials.2013.12.055.

30. Kyriakou I, Dimitris Emfietzoglou V, Ivanchenko MC. *et al*. Microdosimetry of electrons in liquid water using the low-energy models of Geant4. *J Appl Phys* 2017;**122**:024303. https://doi.org/10.1063/1.4992076.

31. Capala J, Makar MS, Coderre JA. Accumulation of boron in malignant and normal cells incubated in vitro with boronophenylalanine, mercaptoborane or boric acid. *Radiat Res* 1996;**146**:554–60. https://doi.org/10.2307/3579556.

32. Hartzell S, Guan F, Taylor P. *et al*. Uncertainty in tissue equivalent proportional counter assessments of microdosimetry and RBE estimates in carbon radiotherapy. *Phys Med Biol* 2021;**66**:155018. https://doi.org/10.1088/1361-6560/ac1366.

33. Böhlen TT, Brons S, Dosanjh M. *et al*. Investigating the robustness of ion beam therapy treatment plans to uncertainties in biological treatment parameters. *Phys Med Biol* 2012;**57**:7983–8004. https://doi.org/10.1088/0031-9155/57/23/7983.

34. Morris G, Smith D, Patel H. *et al*. Boron microlocalization in oral mucosal tissue: implications for boron neutron

capture therapy. *Br J Cancer* 2000;**82**:1764–71. https://doi.org/10.1054/bjoc.2000.1148.

35. International Atomic Energy Agency (IAEA). *Advances in Boron Neutron Capture Therapy*. Non-serial Publications. Vienna: IAEA, 2023.

36. Ishiyama S. Deterministic parsing model of the compound biological effectiveness (CBE) factor for intracellular 10 boron distribution in boron neutron capture therapy. *J Cancer Ther* 2014;**05**:1388–98. https://doi.org/10.4236/jct.2014.514140.

37. Kato I, Ono K, Sakurai Y. *et al.* Effectiveness of BNCT for recurrent head and neck malignancies. *Appl Radiat Isot* 2004;**61**:1069–73. https://doi.org/10.1016/j.apradiso.2004.05.059.

38. Wessol D, Cohen M, Harkin G. *et al. SERA Workshop Lab Manual*. INEEL/EXT-99-00766, 1999.

39. Streitmatter SW, Stewart RD, Moffitt G, Jevremovic T. Mechanistic modeling of the relative biological effectiveness of boron neutron capture therapy. *Cells* 2020;**9**:2302. https://doi.org/10.3390/cells9102302.